Fuel 183 (2016) 170–176

Contents lists available at ScienceDirect

Fuel

journal homepage: www.elsevier.com/locate/fuel

Full Length Article

Hydrogen production from chemical looping steam reforming of glycerol by Ni based Al-MCM-41 oxygen carriers in a fixed-bed reactor

Bo Jiang [a], Binlin Dou [a,*], Kaiqiang Wang [a], Yongchen Song [a], Haisheng Chen [b,*], Chuan Zhang [a], Yujie Xu [b], Mengjue Li [a]

[a] School of Energy and Power Engineering, Key Laboratory of Ocean Energy Utilization and Energy Conservation of Ministry of Education, Dalian University of Technology, 116023 Dalian, China
[b] Institute of Engineering Thermophysics, Chinese Academy of Sciences, Beijing 100190, China

HIGHLIGHTS

- Novel OCs for CLSR were prepared by nanoparticles encapsulated in MCM-41 from MMt.
- Direct-synthesis OCs have well-ordered mesostructure with 4–6 nm nanoparticles.
- Ce in Ni/Al-MCM-41 effectively control particles distribution and enhance OT and WGS.
- Activity and stability of CeNi/Al-MCM-41 for multi-cycles CLSR were found to be high.

GRAPHICAL ABSTRACT

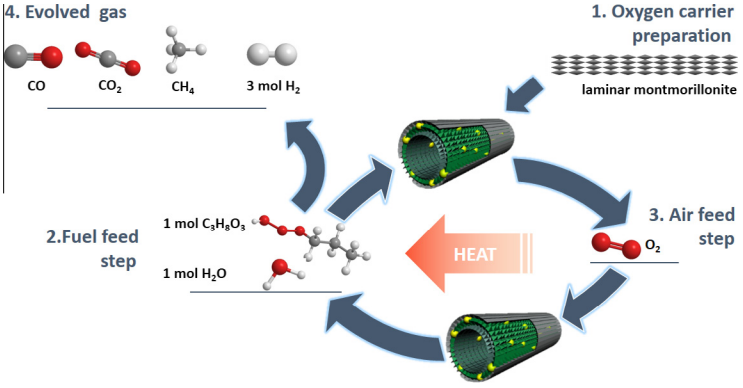

ARTICLE INFO

Article history:
Received 16 December 2015
Received in revised form 12 May 2016
Accepted 11 June 2016
Available online 22 June 2016

Keywords:
CLR
Oxygen carrier
Al-MCM-41
Ceria
Different synthesis method
Montmorillonite

ABSTRACT

This paper describes the synthesis of a series of Ni based Al-MCM-41 oxygen carriers with and without Ce promoter and their application in chemical looping steam reforming of glycerol. The Al-MCM-41 is derived from montmorillonite. The oxygen carriers were prepared by direct-synthesis and post-synthesis method. A variety of technologies including N_2 adsorption-desorption, X-ray diffraction (XRD), inductively coupled plasma optical emission spectroscopy (ICP-OES), H_2 temperature-programmed reduction (H_2-TPR), and transmission electron microscopy (TEM) were conducted to characterize the fresh and used oxygen carriers. The results show the direct-synthesis oxygen carrier possesses excellent textual properties, such as high Ni loading, small particle size, large pore volume, and uniform pore size. The incorporation of Ce could effectively control particle size via strong metal support interaction, promote the homogeneous distribution of Ni, and enhance oxygen mobility capability and water gas shift reaction. And thus shorten 'dead time' during the fuel feed step. The CeNi/Al-MCM-41 displayed the superior activity and excellent long-term stability, which could be due to the strengthened anti-sintering and coke capability.

1. Introduction

Nowadays, hydrogen production from steam reforming biomass attracts lots of interests considering the environmental impact. However, most of these catalysts suffer from deactivation due to the formation of coke or sulphides on the active surface. To

* Corresponding authors.
E-mail addresses: bldou@dlut.edu.cn (B. Dou), chen_hs@mail.etp.ac.cn (H. Chen).

http://dx.doi.org/10.1016/j.fuel.2016.06.061
0016-2361/

overcome this problem, researchers proposed a chemical looping reforming (CLR) progress, in which the catalyst is continuously regenerated by air [1,2]. This is achieved by circulating the oxygen carrier (OC) between a reformer, in which the OC contacts with fuel, and a regenerator, in which the OC and coke deposited are oxidized by air [3]. We recently demonstrated renewable H_2 generation from glycerol via CLR, which was carried out by Ni-based OCs [4]. The autothermal and continuous hydrogen production by CLR in a moving-bed reactor has been investigated in our previous study [5]. The OC in CLR performs a bifunctional material: (1) oxygen transfer medium during redox cycle and (2) steam reforming catalyst in its reduced state. Hence, an excellent OC should be a unique combination of high catalytic activity and splendid redox property.

Previously, researches have focused on different OCs including Mn, Ni, Cu and Fe-based OCs, and concluded that Ni-based OCs may present high reactivity and stability at harsh reaction conditions [6]. However, the major barrier for Ni based OCs is the rapid deactivation caused by coke deposition and metal sintering [7]. It is significant that coke formation on Ni-based OCs strongly depends on the availability of lattice oxygen. A feasible strategy to solve this problem is to add the promoter. It has been reported that CeO_2 has remarkable redox reactions and oxygen storage-release capability by altering state between Ce^{3+} and Ce^{4+} [8]. Moreover, the incorporation of Ce could strengthen the metal-support interaction (MSI) and promote Ni distribution [9]. It is also remarkable that Ni-CeO_2 system shows low methanation activity and high water gas shift (WGS) activity, which is crucial to achieve high selectivity to H_2 in fuel feed step [10]. In addition, an effective approach to improve the Ni dispersion and suppress the sintering of Ni nanoparticles is to accommodate them in porous supports, such as porous silica or alumina. Recently, the preparation of mesoporous materials that are derived from various types of natural layered silicates, such as montmorillonite, has been emphasized because of the abundance of the starting material and the similarity of the natural material's structure units to those of mesoporous material. Encapsulation of inorganic species into these aluminosilicate-mesoporous materials can potentially be used as OCs in CLR. Two approaches, direct-synthesis and post-synthesis method, have been developed to prepare these hybrid ordered mesoporous materials. Both approaches have pros and cons [11].

Considering above strategies, it is expected to develop a Ce promoted Ni based Al-MCM-41 OC for hydrogen generation in CLR. As the OCs synthesized by different methods show different characteristics, it is significant to investigate the effect of synthesis method on the CLR activity and stability.

2. Experimental

2.1. Preparation of OCs

The Al-MCM-41 was synthesized as following steps. Montmorillonite (Aldrich) of 10.0 g was first mixed with 15.0 g NaOH at 600 °C for 2 h, followed by being dispersed in 400 mL deionized water and aged for 16 h at room temperature. The supernatant was employed as Al and Si source in the following steps. Deionized water (50 mL) was used to dissolve 1.0 g CTAB and 1.0 g PEG4000, and then supernatant (Al and Si source) of 80 mL was added into above aforesaid solution under stirring. The mixture was continuously stirred for 1 h at 30 °C. An HCl solution (2 M) was added into the mixture to adjust the pH value to 9. The mixture was vigorously stirred for 1 h at 30 °C, and then transferred into the Teflon-lined steel autoclave. The sample was heated at 110 °C for 24 h and cooled to the room temperature. The resultant was filtered, washed and dried at 80 °C for 12 h, and then calcined at a heating rate of 5 °C/min to 650 °C for 3 h.

CeNi/Al-MCM-41 and Ni/Al-MCM-41 oxygen carrier was prepared by the direct-synthesis method on the basis of Ref. [12] with modifications. The Ni loading was fixed to about 7 wt% for the both samples. The Ce loading was set to about 1 wt% in the sample of CeNi/Al-MCM-41. The synthetic routine was similar to the synthesis of the Al-MCM-41. The difference is that $Ni(NO_3)_3{\cdot}6H_2O$ ($Ce(NO_3)_3{\cdot}6H_2O$ and $Ni(NO_3)_3{\cdot}6H_2O$) dissolved in deionized water with CTAB and PEG4000 was added into the Al and Si source supernatant.

Ni@Al-MCM-41 was prepared by a surfactant-assisted isovolumetric wetness impregnation method (post-synthesis method). The Ni loading was also fixed to about 7 wt% in this sample. The as-prepared Al-MCM-41 was immersed into $Ni(NO_3)_3{\cdot}6H_2O$ solution with the help of CTAB. The resultant was further sonicated for 0.5 h and then dried at 80 °C overnight. Finally, the powder was calcined at 650 °C for 4 h at a heating rate of 5 °C/min.

2.2. Characterization and activity tests

XRD (Shimadzu XRD-600) was applied to determine crystalline phase in the samples and identify the mesoporous structure using graphite filtered Cu Kα radiation (λ = 0.15406 nm). ICP-OES (VISTA-PROAX spectrophotometer) was used to determine the actual elemental content of the metals. N_2 adsorption-desorption analysis (Micromeritics ASAP 2020 Sorptometer) was performed at 77 K and the pore size distributions and the cumulative pore volumes were obtained from desorption branches of the isotherms by Barret-Joyner-Halenda (BJH) method. Morphology of the OCs was obtained by a HRTEM (TECNAI G2 F20) equipped with an energy dispersion X-ray spectrometer (EDS). H_2-TPR was conducted on a Micromeritics Autochem II 2920 instrument so as to analyse metal-support interaction. As testing of OCs in a continuous unit does not allow for the detail resolution of the reduction and oxidation properties of the materials [3]. The activity and stability tests of OCs in CLR of glycerol were evaluated in a down-flow fixed-bed reactor (diameter 12 mm) operating at 650 °C and ambient pressure. The experimental methods and relevant calculations have been reported in our previous studies [4,13].

3. Results and discussion

3.1. Characterization of fresh and spent OCs

The N_2 adsorption-desorption isotherms of fresh OCs are illustrated in Fig. 1(a). All the samples exhibited typical IV behavior with an H1 type hysteresis loop, which is a typical characteristic for mesoporous materials with two-dimensional hexagonal structures. The pore size distribution shown in Fig. 1(b) reveals that CeNi/Al-MCM-41 and Ni/Al-MCM-41 have narrower pore size distribution range, and Ni@Al-MCM-41 loses the uniform pore size distribution indicating that the NiO nanoparticles encapsulated in Ni@Al-MCM-41 may enhance the roughness of the pore wall and/or partially block the mesopores of the matrix. The textural properties of the samples are listed in Table 1. It is pronounced that the incorporation of the active phase has remarkable impact on physical properties of Al-MCM-41, as obvious decrease in the specific surface area and pore volume. The Ni@Al-MCM-41 derived from post-synthesis method possessed smaller surface area and pore volume, compared with Ni/Al-MCM-41 derived from direct-synthesis method. This is mainly due to Ni precursors deposition on the support in the form of a finely dispersed layer in the post synthesis method, which could block the entrance or/and exit of some mesopores [14].

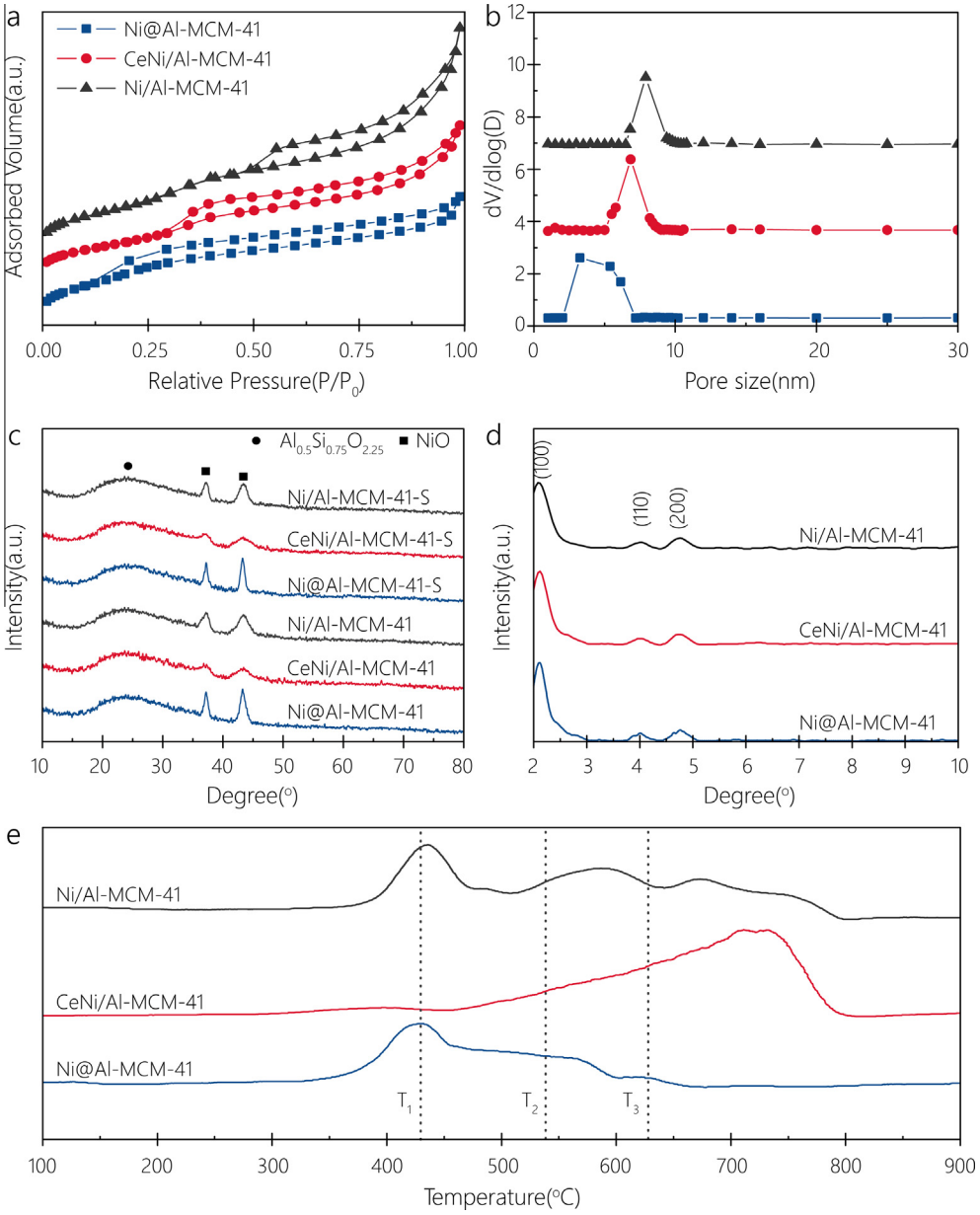

Fig. 1. Characterization of OCs. (a) N_2 adsorption-desorption of fresh OCs, (b) pore size distribution of fresh OCs, (c) full-range XRD profiles of fresh and used OCs, (d) small-angle XRD profiles of fresh OCs, and (e) TPR profiles of fresh OCs.

Full-range XRD patterns of the fresh and used OCs are illustrated in Fig. 1(c). The broad peaks from $2\theta = 18.0–32.0°$ could be assigned to the reflection peaks of the Si-Al frameworks of Al-MCM-41 support for all OCs. After stability tests, Si-Al frameworks have been maintained, indicating that the mesoporous structure possesses high thermal stability. Small-angle XRD patterns of the fresh OCs are shown in Fig. 1(d). All of the three OCs exhibit three well-resolved peaks indexed to (1 0 0), (1 1 0) and (2 0 0) reflections, which are associated to a *p*6 mm hexagonal symmetry. The peaks originated at about 43.3° were the reflection of the (2 0 0) plane of the NiO nanocrystals with a face-centered cubic structure, while the mean NiO crystalline sizes were estimated from this plane (listed in Table 1). Note that no peak corresponding to CeO_2 is observed, revealing that CeO_2 is either amorphous or well dispersed in the OC. The NiO reflection of CeNi/Al-MCM-41 was very weak along with the line broadening, which is responsible for the smaller NiO nanoparticle size in the presence of CeO_2. Gonzalez-DelaCruz et al. [15] have demonstrated that Ni could spread all over Ni-Ce interface and be stabilized by the strong MSI, resulting in high dispersion of Ni, and thus it is conducive to reduce the Ni particle size. Compared with Ni@Al-MCM-41, Ni/Al-MCM-41 shows narrow and sharp peaks, indicating that direct-synthesis method is beneficial to form small NiO crystallites. No graphite peaks are detected for all the used OCs, resulting from the effective coke deposition elimination capability of air feed step. The average NiO crystal sizes of the used OCs decrease in following sequence: Ni@Al-MCM-41, Ni/Al-MCM-41 and CeNi/Al-MCM-41 (listed in Table 1). It is clearly that the Ce promoted OC shows negligible changes after the stability test, indicating excellent anti-sintering performance due to the strong MSI and the confinement of mesoporous structure.

H_2-TPR profiles of the prepared OCs are shown in Fig. 1(e). The sample with high temperature against reduction reflected a strong MSI, which could enhance the thermal stability to suppress

Table 1
Textual properties of samples.

Sample	S_{BET} (m^2/g)	V_{pore} (cm^3/g)	Ni content (wt%)[a]	Ce content (wt%)[a]	D_{NiO} (nm)[b]	D_{NiO} (nm)[c]	S_H (m^2/g_{Ni})[d]
Al-MCM-41	1104.21	0.81	–	–	–	–	–
Ni@Al-MCM-41	907.26	0.55	5.08	–	8.44	14.01	9.6
CeNi/Al-MCM-41	848.40	0.58	6.59	2.51	6.05	6.28	16.5
Ni/Al-MCM-41	938.45	0.60	7.05	–	5.47	9.19	13.4

[a] Determined by ICP-OES.
[b] Calculated from Scherrer's equation from the (2 0 0) plane of NiO in XRD from the fresh oxygen carrier.
[c] Calculated from Scherrer's equation from the (2 0 0) plane of NiO in XRD from the oxygen carrier after the air feed step.
[d] Nickel active surface area determined by H_2 pulse chemisorption.

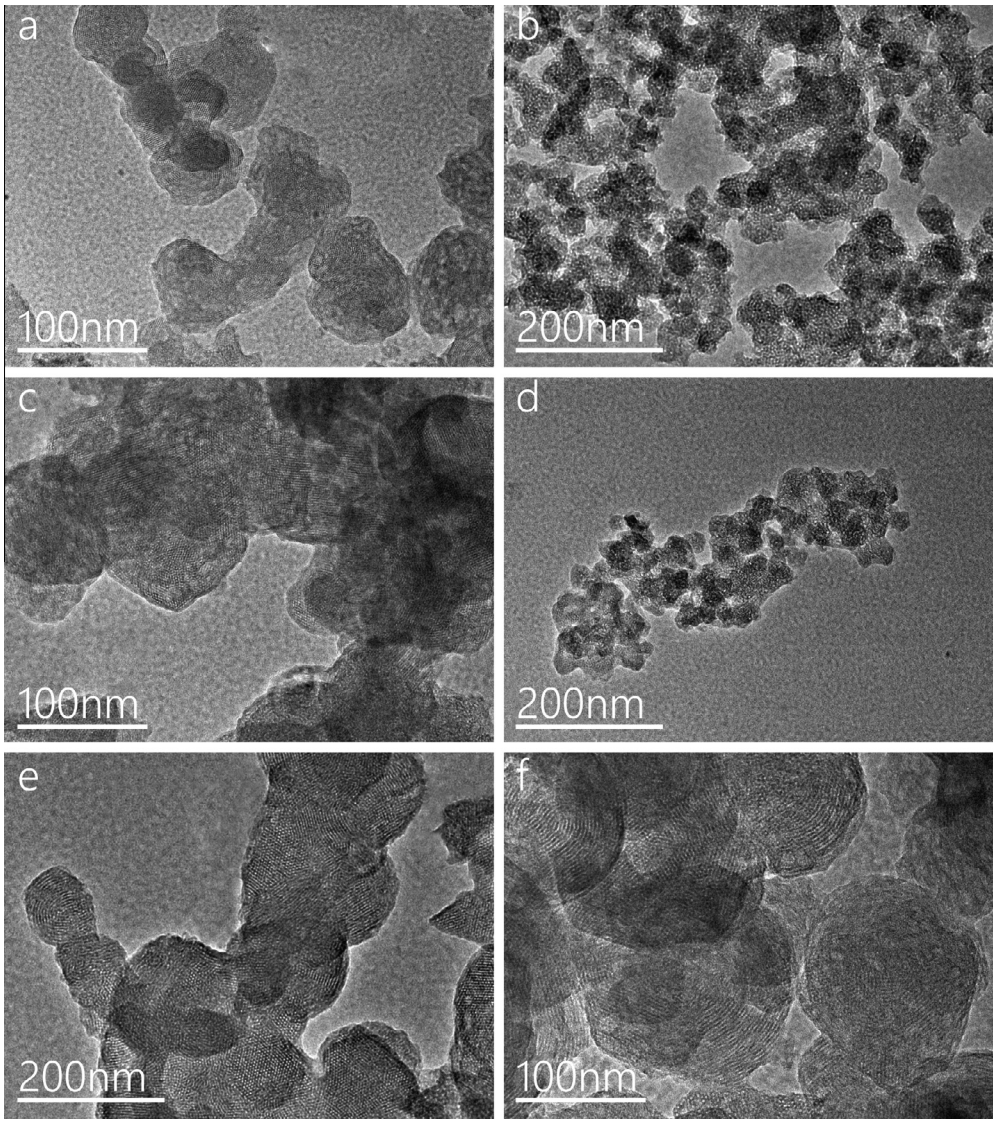

Fig. 2. TEM profiles of fresh and used OCs. (a) Fresh Ni@Al-MCM-41, (b) used Ni@Al-MCM-41, (c) fresh Ni/Al-MCM-41, (d) used Ni/Al-MCM-41, (e) fresh CeNi/Al-MCM-41 and (f) used CeNi/Al-MCM-41.

sintering. Three reduction peaks are observed for fresh OCs. According to previous investigations, Ni^{2+} is reduced to Ni^0 without going through intermediate oxides. Thus, the three H_2 consumption peaks should be assigned to different Ni species. For the Ni@Al-MCM-41 sample, three reduction peaks were detected at 410, 550 and 620 °C, respectively. The sharp peak originated at 410 °C is resulted from the reduction of the bulk NiO located on the external surface in a weak interaction with the support, while the second reduction peak centered at 550 °C should be caused by the reduction of the NiO species in the interior of the silica wall which is less reducible due to strong metal-support interaction [16]. The last reduction peak at 620 °C could be assigned to the reduction of the NiO in the subsurface, indicating the formation of the nickel phyllosilicate [17]. Over the Ni/Al-MCM-41, a main peak and two shoulders were found, which were assigned to different locations of Ni ions. Compared with Ni@Al-MCM-41, all three

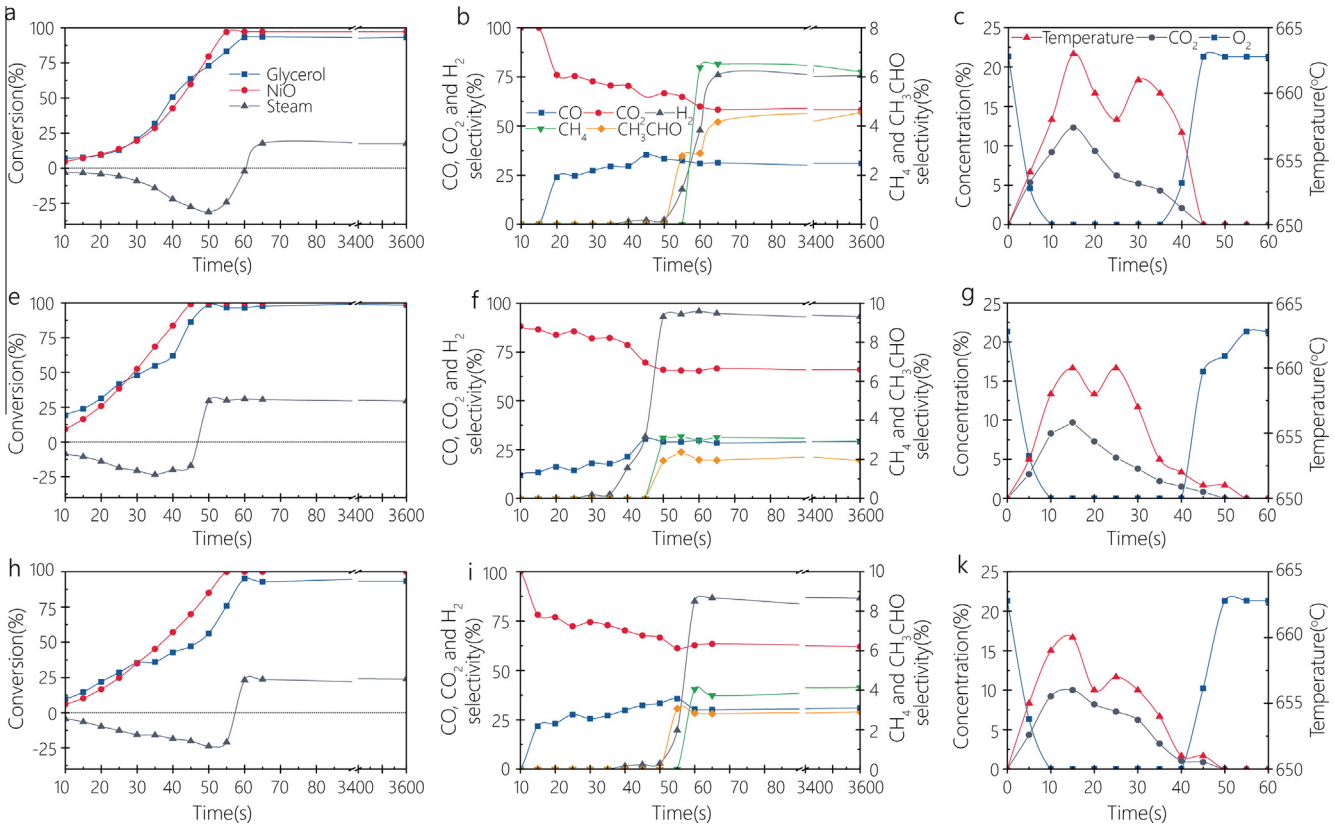

Fig. 3. Activity test results of three OCs. Ni@Al-MCM-41: (a) conversions vs time in fuel feed step, (b) selectivity vs time in fuel feed step and (c) CO_2, O_2 and temperature varieties in air feed step; CeNi/Al-MCM-41: (a) conversions vs time in fuel feed step, (b) selectivity vs time in fuel feed step and (c) CO_2, O_2 and temperature varieties in air feed step; Ni/Al-MCM-41: (a) conversions vs time in fuel feed step, (b) selectivity vs time in fuel feed step and (c) CO_2, O_2 and temperature varieties in air feed step. (N_2 purge steps are not shown in this figure.)

reduction peaks shifted towards higher temperatures, indicating the stronger interaction with silica matrix for the three NiO species. The lower reducibility extent is due to the better confinement effect of the direct-synthesis method. On the other hand, the domains of integration related to the H_2 consumption of the second and third reduction peaks were larger. It can be suggested that most of the Ni ions is either highly dispersed in the interior of the silica wall or incorporated into the silica framework. After the introduction of the second metal Ce, some changes occurred in the TPR profiles. A broad peak in the range from 400 °C to 750 °C was observed. It could be divided into two peaks by deconvolution. Thus, there actually are three NiO peaks in CeNi/Al-MCM-41. The intensity of the first reduction peak (380 °C) is inconspicuous, while the latter two (400–700 °C) show high intensity. This indicates few NiO is adsorbed on the external surface and the decrease of reducibility of NiO on the internal surface and subsurface in the presence of Ce is due to the metal synergistic effect [18].

TEM images of OCs are displayed in Fig. 2. Obviously, the highly ordered structure is retained after the calcination and stability tests for all OCs. This observation indicates the ordered mesoporous structure reveals excellent thermal stability. The hexagonal structure is clearly observed in three OCs images with the electron beam parallel to the pore direction. Moreover, the images with the electron beam perpendicular to the pores demonstrate the OCs possess long-range order and a regular two-dimensional hexagonal pore structure, corresponding to the intense XRD peaks at low angles and the H1 type hysteresis loops in N_2 adsorption-desorption isotherms. All the fresh OCs show no apparent nanoparticles in TEM images, and this suggests that NiO and CeO_2 nanoparticles are highly dispersed throughout the whole structure [19]. After the stability test, no OC presented coke deposition on the surface. This indicates the air feed step could completely eliminate coke deposition after every individual fuel feed step. CeNi/Al-MCM-41 still preserved high nanoparticle dispersion, however, for the other two OCs, NiO nanoparticles appeared to migrate to external surface of the support at different extent. This migrating NiO particle might be derived from: (1) the aggregation of some NiO from the destroyed framework; (2) small NiO nanoparticles migrated out of internal surface because of relative weak metal-support interaction during the air feed step [20].

3.2. Activity and stability tests of OCs

As shown in Fig. 3, it is significant that H_2 production is delayed for all OCs. It could be attributed to the reduction of NiO to Ni at the initial stage of fuel feed step. In other words, the steam reforming reaction would not completely occur until NiO is converted into Ni at the maximum extent (Fig. 3(a), (e) and (h)). At the 'dead time', a significant negative steam conversion occurred for all of the OCs. This is caused by the H_2O formation in this period [4]. It is a further evidence of the NiO reduction by fuel. Upon upscaling process, the 'dead time' would cause exaggerated intermittency in H_2 generation. It is worthy of nothing that the 'dead time' decreases in the following sequence: Ni@Al-MCM-41, Ni/Al-MCM-41 and CeNi/Al-MCM-41. This sequence is corresponding with the variety of active surface area of these OCs (listed in Table 1). Considering the proposed reaction mechanism of 'dead time' [21], we have reason to believe that the duration of the 'dead time' is closely related to the dispersion of the active phase. Thus, we can conclude that the direct-synthesis method and Ce promoter are conducive to shorten the 'dead time'. At the end of 'dead time', it is clearly that all the measurement parameters change significantly. At the

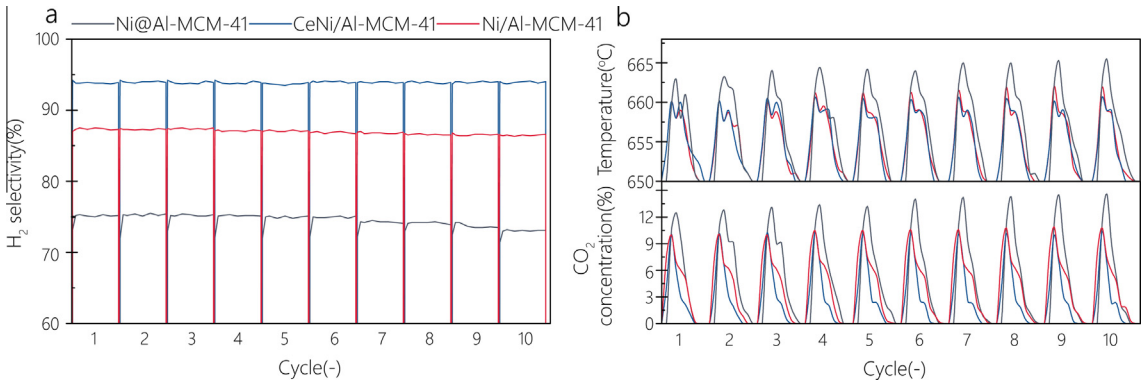

Fig. 4. Stability tests of three OCs. (a) H_2 selectivity during the fuel feed step, (b) CO_2 concentration and temperature varieties during the air feed step.

steady stage, all OCs reach glycerol conversion above 80%, and hydrogen selectivity is up to 75%. The glycerol conversion and H_2 selectivity decrease in this order: CeNi/Al-MCM-41, Ni/Al-MCM-41, and Ni@Al-MCM-41. This could be associated with active nickel surface area, as Ni is identified as the active center for C—C and C—H bond cleavage, which facilitates the conversion of glycerol and C_2 intermediate. The CH_4 selectivity for all the OCs investigated is not high, indicating that methanation is inhibited under this reaction condition because of its extremely exothermic nature. Since CO_2/CO ratio is considered as an indicator of WGS activity, the higher H_2 selectivity with Ce addition is probably related to the promotion of WGS reaction. As shown in Fig. 3(c), (g) and (k), all of the OCs exhibit significant temperature rise which is caused by coke and Ni oxidation. The CO_2 peak area corresponds to the amount of coke deposition during the fuel feed step. It is clearly that CeNi/Al-MCM-41 exhibit smallest peak area. It indicates that the Ce promoter could effectively suppress the coke formation in the fuel feed step. The final stage of air feed step was signaled by sharp rise of O_2 concentration from 0% to 23%. This suggests the complete replenishment of OCs and elimination of coke.

As shown in Fig. 4(a), it is significant that the CeNi/Al-MCM-41 and Ni/Al-MCM-41 shows more steady H_2 selectivity during 10 cycles, compared with Ni@Al-MCM-41. The superior stability of the direct-synthesis sample is reasonable because most of inorganic precursors tend to be adsorbed on internal surface or subsurface rather than external surface in the direct-synthesis process. This would enhance the confinement effect, thus effectively suppress sintering. All the three oxygen carriers possessed high tolerability during 10 cycle tests, indicating that air feed step could effectively clean the carbon deposition from the surface of OCs. The temperature rise and amount of CO_2 of Ni@Al-MCM-41 and Ni/Al-MCM-41 increase with the proceeding of the tests. This could be caused by the growth of Ni nanoparticles. Chen et al. [22] have demonstrated that small Ni crystals possesses a high saturation concentration of coke and therefore a low driving force for coke diffusion through the nickel crystals. As a consequence, the gradual sintering of Ni would exacerbate the coke deposition issue simultaneously. The addition of Ce improve the MSI and thus enhance the sintering resistance. So CeNi/Al-MCM-41 showed steady temperature variety and CO_2 concentration at the stability test.

4. Conclusions

Three nickel nanoparticles encapsulated inside Al-MCM-41, derived from montmorillonite, mesoporous OCs were successfully synthesized via different synthesis method, and for the first time used in CLR progress. It is clear that both ordered mesoporous structure and Ce promoter play important role in achieving excellent CLR performance. The OCs derived from direct-synthesis method could improve Ni loading, dispersion and MSI, and the Ce modification could effectively control the size of nickel size, improve the reducibility of partial NiO species, and promote WGS reaction. The synergistic effect of above results lead to the high activity, good stability and short 'dead time'.

Acknowledgement

This work is supported by the Natural Science Foundation of China (Project Nos. 91434129 and 51476022). This work was also supported by International Science and Technology Cooperation Program of China (2014DFA60600) and Dalian (2015F11GH091), and the Fundamental Research Funds for the Central Universities (DUT15JJ(G)02).

References

[1] Lind F, Seemann M, Thunman H. Continuous catalytic tar reforming of biomass derived raw gas with simultaneous catalyst regeneration. Ind Eng Chem Res 2011;50:11553–62.
[2] Keller M, Leion H, Mattisson T. Chemical looping tar reforming using La/Sr/Fe-containing mixed oxides supported on ZrO_2. Appl Catal B – Environ 2016;183:298–307.
[3] Keller M, Leion H, Mattisson T. Use of $CuO/MgAl_2O_4$ and $La_{0.8}Sr_{0.2}FeO_3$/gamma-Al_2O_3 in chemical looping reforming system for tar removal from gasification. AIChE J 2016;62:38–45.
[4] Jiang B, Dou BL, Song YC, Zhang C, Du BG, Chen HS, et al. Hydrogen production from chemical looping steam reforming of glycerol by Ni-based oxygen carrier in a fixed-bed reactor. Chem Eng J 2015;280:459–67.
[5] Dou BL, Song YC, Wang C, Chen HS, Yang MJ, Xu YJ. Hydrogen production by enhanced-sorption chemical looping steam reforming of glycerol in moving-bed reactors. Appl Energy 2014;130:342–9.
[6] Adanez J, Abad A, Garcia-Labiano F, Gayan P, de Diego LF. Progress in chemical looping combustion and reforming technologies. Prog Energy Combust Sci 2012;38:215–82.
[7] Tang M, Xu L, Fan M. Progress in oxygen carrier development of methane-based chemical-looping reforming: a review. Appl Energy 2015;151:143–56.
[8] Zhang CX, Li SR, Li MS, Wang SP, Ma XB, Gong JL. Enhanced oxygen mobility and reactivity for ethanol steam reforming. AIChE J 2012;58:516–25.
[9] Li D, Zeng L, Li X, Wang X, Ma H, Assabumrungrat S, et al. Ceria-promoted Ni/SBA-15 catalysts for ethanol steam reforming with enhanced activity and resistance to deactivation. Appl Catal B – Environ 2015;176–177:532–41.
[10] Ang ML, Oemar U, Saw ET, Mo L, Kathiraser Y, Chia BH, et al. Highly active Ni/xNa/CeO_2 catalyst for the water gas shift reaction: effect of sodium on methane suppression. ACS Catal 2014;4:3237–48.
[11] Zhang WH, Lu XB, Xiu JH, Hua ZL, Zhang LX, Robertson M, et al. Synthesis and characterization of bifunctionalized ordered mesoporous materials. Adv Funct Mater 2004;14:544–52.
[12] Huo CL, Ouyang J, Yang HM. CuO nanoparticles encapsulated inside Al-MCM-41 mesoporous materials via direct synthetic route. Sci Rep-UK 2014;4:9.
[13] Jiang B, Dou B, Wang K, Zhang C, Song Y, Chen H, et al. Hydrogen production by chemical looping steam reforming of ethanol using NiO/montmorillonite oxygen carriers in a fixed-bed reactor. Chem Eng J 2016;298:96–106.
[14] Calles JA, Carrero A, Vizcaino AJ, Garcia-Moreno L. Hydrogen production by glycerol steam reforming over SBA-15-supported nickel catalysts: effect of alkaline earth promoters on activity and stability. Catal Today 2014;227:198–206.

[15] Gonzalez-DelaCruz VM, Holgado JP, Pereniguez R, Caballero A. Morphology changes induced by strong metal-support interaction on a Ni-ceria catalytic system. J Catal 2008;257:307–14.
[16] Liu D, Quek XY, Cheo WNE, Lau R, Borgna A, Yang Y. MCM-41 supported nickel-based bimetallic catalysts with superior stability during carbon dioxide reforming of methane: effect of strong metal-support interaction. J Catal 2009;266:380–90.
[17] Vizcaíno AJ, Carrero A, Calles JA. Hydrogen production by ethanol steam reforming over Cu-Ni supported catalysts. Int J Hydrogen Energy 2007;32:1450–61.
[18] Carrasco J, Barrio L, Liu P, Rodriguez JA, Ganduglia-Pirovano MVn. Theoretical studies of the adsorption of CO and C on Ni (1 1 1) and Ni/CeO_2(1 1 1): evidence of a strong metal-support interaction. J Phys Chem C 2013;117:8241–50.
[19] Ma HY, Zeng L, Tian H, Li D, Wang X, Li X, et al. Efficient hydrogen production from ethanol steam reforming over La-modified ordered mesoporous Ni-based catalysts. Appl Catal B – Environ 2016;181:321–31.
[20] Wang N, Xu Z, Deng J, Shen K, Yu X, Qian W, et al. One-pot synthesis of ordered mesoporous NiCeAl oxide catalysts and a study of their performance in methane dry reforming. ChemCatChem 2014;6:1470–80.
[21] Fermoso J, Gil MV, Rubiera F, Chen D. Multifunctional Pd/Ni-Co catalyst for hydrogen production by chemical looping coupled with steam reforming of acetic acid. ChemSusChem 2014;7:3063–77.
[22] Chen D, Christensen KO, Ochoa-Fernández E, Yu Z, Tøtdal B, Latorre N, et al. Synthesis of carbon nanofibers: effects of Ni crystal size during methane decomposition. J Catal 2005;229:82–96.